RAPID COMMUNICATIONS

PHYSICAL REVIEW A VOLUME 43, NUMBER 4 15 FEBRUARY 1991

Phase modulation of Taylor vortex flow

Mingming Wu and C. David Andereck
Department of Physics, The Ohio State University, Columbus, Ohio 43210
(Received 5 November 1990; revised manuscript received 26 December 1990)

The phase dynamics of Taylor vortex flow close to onset was studied by applying a forced modulation to the upper boundary of a large-aspect-ratio concentric-cylinder system. Our experimental results show that the phase disturbances progress diffusively along the Taylor vortices in the axial direction. Values of the diffusion coefficients obtained experimentally are compared with those found in numerical computations. We also confirm the dependence of the diffusion coefficient on the wave vector of the Taylor vortices predicted by the general theoretical model of Pomeau and Manneville [J. Phys. (Paris) Lett. **40**, L609 (1979)].

In the last decade, much attention has been given to the phase dynamics of patterns in hydrodynamic systems where the transition from a uniform state to a spatially periodic state occurs.[1-5] One of the classic examples is the Taylor-Couette system, which consists of fluid between two concentric cylinders with the inner one rotating. When the rotation frequency of the inner cylinder exceeds a threshold value, the spatially uniform circular Couette flow (CCF) changes to the axially periodic Taylor vortex flow (TVF). The flow pattern undergoes successive transitions as the inner cylinder rotation frequency increases further, leading eventually to turbulent flow. The characteristics of the flows in the Taylor-Couette system have been investigated extensively by visualizing the patterns and measuring the velocity profiles.[6] While the Navier-Stokes equation, in principle, provides a theoretical basis for understanding the experimental results,[7,8] the complexity of the equation often makes it difficult to compare with real laboratory situations, therefore necessitating the use of model equations. In particular, dynamics of patterns may be well reproduced with simplified model equations such as the Ginzburg-Landau equation.[9] In this spirit, it has been shown that phase variables (which might be associated with, for instance, the positions of rolls in the Taylor-Couette system) are governed by a simple diffusion equation[1] in the nonequilibrium systems that show spatially periodic structures after a supercritical bifurcation. This provides us with a very simple and direct way to study the slow, long-wavelength dynamics of Taylor vortices with theoretical understanding.

We have performed a detailed experimental study of the phase dynamics near the onset of TVF in a large-aspect-ratio concentric-cylinders system. The phase-diffusion coefficients were obtained by studying the responses of the Taylor vortices to the motion in the axial direction of the top boundary of the system. Two different boundary conditions were implemented in our experiments. In the first case the top boundary oscillated in the axial direction, while in the second case it was moved at a constant speed to a final position. In both cases the pattern disturbances traveled diffusively away from the boundary in the axial direction. The diffusion coefficients we obtained are consistent with the results of numerical computations[10,11] based on the Navier-Stokes equation. We also present experimental results on the dependence of the phase-diffusion coefficient on the wave vector of the Taylor vortices. We found that the diffusion coefficient decreased as the wave vector of the TVF deviated from q_c, the critical wave vector for TVF.[12] These results are consistent with the phase-diffusion model.[1]

The control parameter for the Taylor-Couette system with the outer cylinder at rest is the Taylor number T. It is defined as $T=(\Omega_i r_i d/\nu)(d/r_i)^{1/2}$, where Ω_i is the inner cylinder rotation frequency, r_i is the inner cylinder radius, d is the gap between the inner and outer cylinders, and ν is the kinematic viscosity. When T exceeds the threshold T_c, the flow changes from a uniform CCF to a periodic TVF. In the vicinity of T_c, the lowest order of, for example, the radial velocity field has the form $u(r,z,t)=A(z,t)e^{iq_c z}u(r)$, where $u(r)$ is the eigenfunction, z is the axial position, and q_c is the critical wave vector corresponding to the lowest T_c.[12] The amplitude $A(z,t)$ can then be rewritten as $|A(z,t)|e^{i\phi(z,t)}$, where $\phi(z,t)$ is the phase variable associated with the slow space and time variations in A. ϕ has been predicted[3] to obey a diffusion equation

$$\frac{\partial\phi}{\partial t}=D_{\parallel}\frac{\partial^2\phi}{\partial z^2} \tag{1}$$

where

$$D_{\parallel}=\frac{\xi_0^2}{\tau_0}\frac{(\epsilon-3\xi_0^2q^2)}{(\epsilon-\xi_0^2q^2)}, \tag{2}$$

and τ_0 is the perturbation amplitude growth rate, ξ_0 is the correlation length, $\epsilon=(T-T_c)/T_c$ is the distance to the onset of TVF, $q=\tilde{q}-q_c$, $\tilde{q}$ is the wave vector of the TVF.

Our experiment is conducted in concentric cylinders with the outer one fixed. The inner cylinder radius $r_i=5.262$ cm, the outer cylinder radius $r_0=5.965$ cm, the length between collars initially is 49.5 cm, and therefore the radius ratio $\eta=0.882$ and the aspect ratio $\Gamma=L/(r_0-r_i)=70.4$. The inner cylinder is driven by a Compumotor stepper motor. The working fluid is a solution of double distilled water and 44% glycerol by weight. 1% by volume of Kalliroscope AQ1000 is added for visualization. The forced modulation is added through moving the top collar of the system [see Fig. 1(a)]. A stepper motor can move the collar a maximum distance of 1 cm. The visualized TVF pattern is viewed with a 512×480 pixel CCD

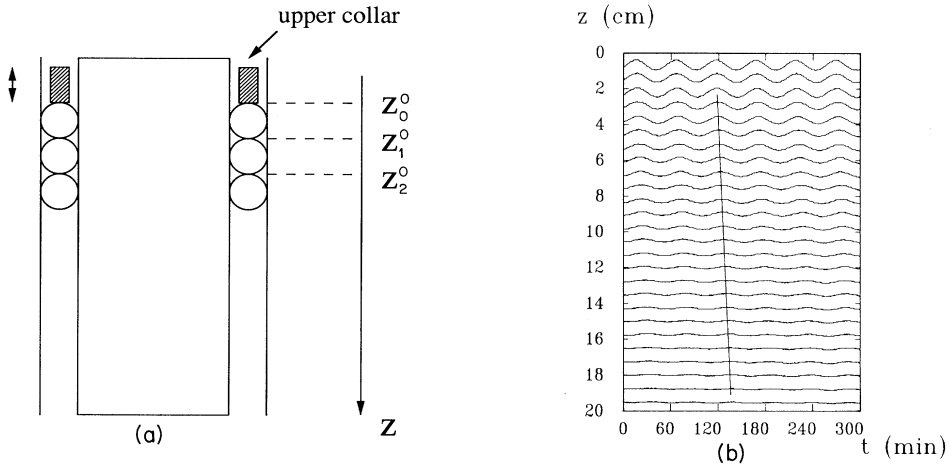

FIG. 1. (a) Schematic diagram of the experimental geometry. (b) Node line locations of TVF subjected to the periodic boundary modulation, t represents time and z is the distance from the top collar. The solid line traces the shift in phase from vortex to vortex.

camera which is connected to an image processor. The light intensity of a vertical line of the pattern is recorded and the positions of the node lines are determined by finding minima of the light intensity profile. For a typical situation we have a resolution of 34 pixels per vortex.

In the first type of experiment, the top collar oscillated in the axial direction. We found that the phase at $z=0$ exactly follows the top collar's motion due to the fact that the period of the modulation $T \gg d^2/\nu$, the diffusion time through a vortex. (Typically, $T=3040$ s and $d^2/\nu=12.3$ s.) This provided the following boundary condition

$$\phi|_{z=0}=\phi_0 \sin(\omega t) . \tag{3}$$

Here ϕ_0 and ω are the modulation amplitude and frequency. Solving Eq. (1) with the above boundary condition, we obtain

$$\phi(z,t)=\phi_0 e^{-\alpha z}\sin(\omega t-\beta z) , \tag{4}$$

$$\alpha=\beta=\left[\frac{\omega}{2D_{\parallel}}\right]^{1/2} . \tag{5}$$

Assuming z_n is the location of the nth vortex node line, then $\phi(z_n,t)+\tilde{q}z_n=n\pi$, therefore

$$\begin{aligned} z_n &= [n\pi-\phi_0 e^{-\alpha z}\sin(\omega t-\beta z)]/\tilde{q} \\ &\simeq z_n^0-\phi_0 e^{-\alpha z_n^0}\sin(\omega t-\beta z_n^0)/\tilde{q} , \end{aligned} \tag{6}$$

where z_n^0 is the location of the vortex node line without modulation and $z_n^0=n\pi/\tilde{q}$. Equation (6) shows that the node lines oscillate sinusoidally, their amplitudes decrease along the axial direction, and a phase shift occurs between the neighboring node line motions.

In the second experiment, we moved the top collar to a final position at a constant speed, which leads to the approximate boundary condition

$$\phi|_{z=0}=\phi_0 H(t) . \tag{7}$$

Here $H(t)$ is the step function, 0 for $t<0$, 1 for $t\geq 0$. It deviates from the real boundary condition owing to the finite time (typically 48 s) for the collar to reach its final position, but our analysis showed that this deviation is negligible in the region far from the boundary (three or

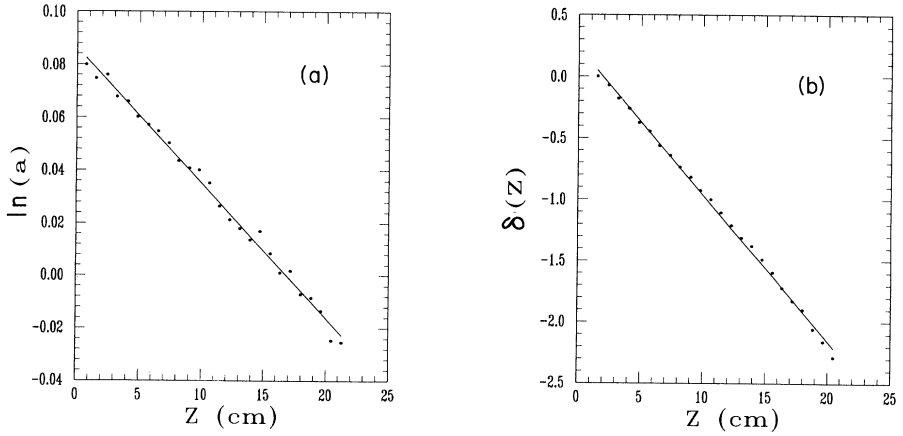

FIG. 2. Dots represent the experimental data and the solid lines are derived from the fit to the diffusion model. (a) a is the amplitude of each node line motion. (b) δ is the phase shift of the node line motion.

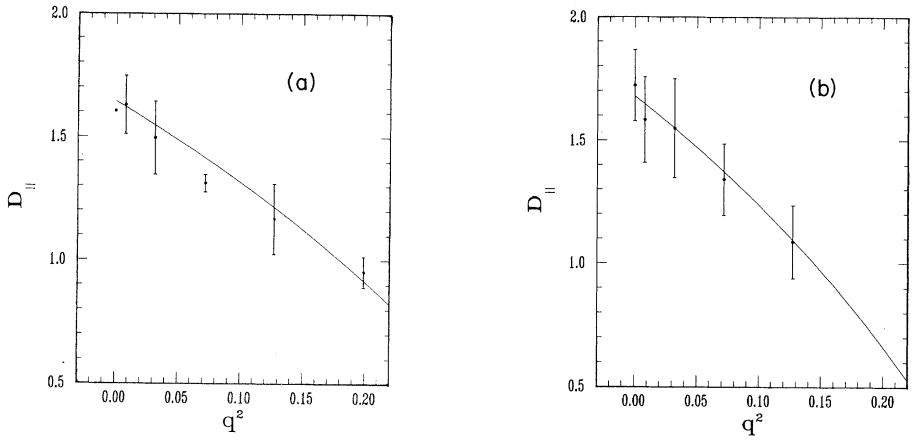

FIG. 3. Relation between $D_{\|}$ and the square of the wave vector, q^2, for: (a) the periodic modulation case; (b) the step-function modulation case. Dots represent the experimental data and the solid lines are the fits to Eq. (2).

more vortices away from the collar). Substituting the above boundary condition in Eq. (1) and following the same procedure as described for the periodic modulation, we find that the location of the nth vortex node line is given by

$$z_n = z_n^0 - d_0 \operatorname{erfc}\left(\frac{z_n}{2(D_{\|}t)^{1/2}}\right) \simeq z_n^0 - d_0 \operatorname{erfc}\left(\frac{z_n^0}{2(D_{\|}t)^{1/2}}\right), \quad (8)$$

where d_0 is the distance that the top collar moves and erfc is the error function complement.

In the periodic modulation case, the sinusoidal motion of the upper collar has a typical amplitude of $d_0/d = 0.480$ and a period of 3040 s. For each set of data, the inner cylinder rotation frequency is adjusted to the TVF region and left about 1 h (our measurements showed that it took about 30 min for our system to reach a steady state). Two hours after starting the modulation, we began recording a vertical line image of the flow pattern every 2 min for 5 h. Figure 1(b) is a typical data set. The response of each node line is a sinusoidal function of time, with an amplitude and phase shift as predicted by Eq. (6). By fitting this data set with the following equation

$$z_n = z_n^0 - a\sin(\omega t - \delta), \quad (9)$$

where a and δ are the amplitude and the phase of the node line motion, we found that $\ln a$ and δ were linearly related to z_n^0 as shown in Fig. 2(a) and 2(b). The slopes of the lines give us values of α and β from Eq. (6), and hence the value of $D_{\|}$. The variations of α and β were within 20%. The resultant value of $D_{\|}$ was found to be independent of the modulation period. Repeating the experiment with a different Taylor vortex wave vector we found that $D_{\|}$ decreased when the wave vector q deviated from q_c. Figure 3(a) shows a typical dependence of $D_{\|}$ on q. The correlation length ξ_0 and correlation time τ_0 can be obtained by fitting this with Eq. (2). The values for this case are listed in Table I.

In the step function case, the upper collar moves at a constant speed (about 0.125 mm/s) to a final position in 48 s, which leads to an aspect ratio increase of 0.853. The response time of each vortex increased with distance of the vortex from the top boundary. For instance, the relaxation time for the 2nd vortex boundary to reach halfway to its steady-state position is 31.1 s after the collar comes to rest, while that of the 3rd vortex boundary is 71.9 s. In this case, the approximation of Eq. (7) is valid for the vortices beyond the three adjacent to the collar. The same data acquisition technique is used here. The light intensity profile of a vertical line is recorded every 12 s after the modulation is added. A typical data set took 40 min. Figure 4 shows a sample result. Fitting this data with the equation

$$z_n = z_n^0 - d_0 \operatorname{erfc}\left(\frac{s_n}{\sqrt{t}}\right), \quad (10)$$

TABLE I. Values of $D_{\|}$ from our experiments, for $\tilde{q} = 3.25$ and $\eta = 0.882$; calculated values of ξ_0 and τ_0 for $\eta = 0.90$ from Ref. 10; and $D_{\|}$ for $\tilde{q} = 3.30$ and $\eta = 0.85$ from Ref. 11.

$D_{\|}$	ξ_0	$1/\tau_0$	ϵ	Source of data
1.63 ± 0.12	0.260	24.3	0.0740	periodic modulation
1.59 ± 0.07	0.293	18.9	0.0740	periodic modulation
1.54 ± 0.20	0.288	19.3	0.0621	constant modulation
1.58 ± 0.17	0.301	17.4	0.0829	constant modulation
	0.382	13.109		Ref. 10
1.70			0.070	Ref. 11

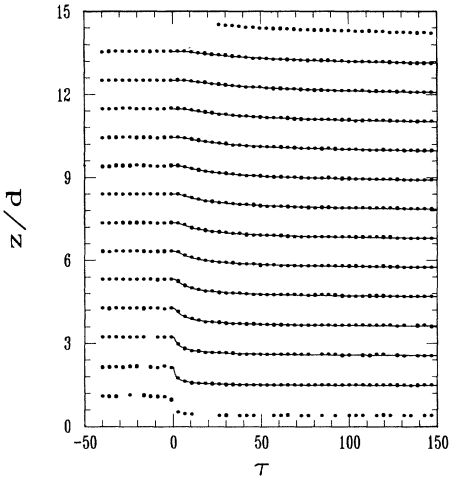

FIG. 4. Node line locations of TVF subjected to the step-function boundary modulation. Modulation is added at $\tau=0$ $[\tau=t/(d^2/\nu)]$. Dots represent the experimental data and solid lines are the error function fits to the data.

where $s_n=z_n^0/2(D_\parallel)^{1/2}$ according to Eq. (8), we obtain s_n as a linear function of z_n^0. Therefore, $D_\parallel$ is evaluated by the slope of s_n and z_n^0. Repeating this process for different TVF wave vectors, we obtained a relation between $D_\parallel$ and wave vector similar to that found in the case of periodic modulation. The results are shown in Fig. 3(b). The resultant values of ξ_0 and τ_0 are shown in Table I in comparison with those from the periodic cases and numerical computations.[10,11] Our values of ξ_0 and τ_0 differ from the numerical values of Ref. 10, while $D_\parallel$ from Ref. 11 is within our error bars for three cases. In both numerical cases, the geometry studied was similar to ours. That we differ with Ref. 10 suggests we may be operating somewhat beyond the range of applicability of Eq. (2), which is, strictly, only appropriate for $\epsilon\rightarrow 0$. Further experiments with ϵ smaller than 0.06 would be needed to verify this.

As shown in Fig. 3(a) and 3(b), the range of wave vectors accessible to us is limited due to the large radius ratio of our system. According to the Eckhaus theory,[12] there are larger stable wave-vector regions of TVF in a small radius ratio system, since it is possible to go to higher ϵ before reaching a wavy instability. Therefore, it is expected that an experiment in a small radius ratio system will show a more profound dependence of $D_\parallel$ upon the wave vector.

In summary, our experimental results have confirmed the basic features of the phase diffusion model proposed by Pomeau and Manneville[1] near the onset of TVF. We studied the phase-diffusion process under two distinct types of modulation and obtained consistent results. In both cases, the phase variables diffused along the Taylor vortices in the axial direction. The measured diffusion coefficients decreased when the Taylor vortex wave vector deviated from q_c.

We express our special thanks to Innocent Mutabazi for many useful discussions. We also thank Doug Dolfinger for developing the modulation apparatus. This work was supported by the Office of Naval Research, under Contract No. N00014-86-K-0071 and Grant No. N00014-89-J-1352.

[1] Y. Pomeau and P. Manneville, J. Phys. (Paris) Lett. **40**, L609 (1979).

[2] J. E. Wesfreid and V. Croquette, Phys. Rev. Lett. **45**, 634 (1980).

[3] P. Tabeling, J. Phys. Lett. **44**, 665 (1983).

[4] H. Brand and M. C. Cross, Phys. Rev. A **27**, 1237 (1983).

[5] M. Lucke and D. Roth, Z. Phys. B **78**, 147 (1990).

[6] H. L. Swinney and R. DiPrima, in *Hydrodynamic Instabilities and the Transition to Turbulence,* 2nd ed., edited by H. L. Swinney and G. P. Gollub (Springer, Berlin, 1985), p. 139.

[7] P. S. Marcus, J. Fluid Mech. **146**, 45 (1984).

[8] P. S. Marcus, J. Fluid Mech. **146**, 65 (1984).

[9] A. C. Newell, J. A. Whitehead, J. Fluid Mech. **38**, 279 (1969). For application to the Taylor-Couette system see R. Graham and J. A. Domaradzki, Phys. Rev. A **26**, 1572 (1982), and references therein.

[10] M. A. Dominguez-Lerma, G. Ahlers, and D. S. Cannell, Phys. Fluids **27**, 856 (1984).

[11] H. Riecke (private communication); see also a related paper, H.-G. Paap and H. Riecke (unpublished).

[12] G. Ahlers, D. S. Cannell, and M. A. Dominguez-Lerma, Physica **23D**, 202 (1986).